AIAA JOURNAL
Vol. 47, No. 2, February 2009

Sound Radiation from a Bypass Duct with Bifurcations

Xiaoxian Chen,* Xun Huang,† and Xin Zhang‡
University of Southampton, Southampton, England SO17 1BJ, United Kingdom

DOI: 10.2514/1.39710

The influence of bifurcations in an aeroengine bypass duct on noise radiation was investigated through high-order-accurate three-dimensional numerical simulations. The physical process was described by a set of acoustic perturbation equations. Four bifurcation arrangements with an airfoil cross section were regularly placed in circumferential direction. Results were compared with those of an axisymmetric duct case without the installation of bifurcations. Both near-field propagation and far-field radiation were studied to show that the bifurcations scatter acoustic modes and redirect sound propagation levels. Compared to the axisymmetric duct case, there are a couple of decibel increases in sound pressure level on some angles due to the installation of bifurcations. The method is also applicable to other configurations with different bifurcations and modes.

Nomenclature

C_0	=	sound speed
k	=	single angular frequency
l, s	=	integer numbers
m, n	=	circumferential and radial modes
p	=	pressure
r	=	radial distance
t	=	sound wave propagation time
u, v, w	=	velocity in cylindrical coordinates
x, y, z	=	Cartesian coordinates
α	=	angle between two torque links
θ	=	circumferential angle
λ	=	sound wavelength
ϕ	=	radiation angle

Subscripts

m, n	=	circumferential mode and radial mode
0	=	background flow value

Superscript

$'$	=	acoustic disturbance value

I. Introduction

ENGINE noise is an important component of aircraft noise generated by the takeoff and approach to landing of aircraft. For engines with a high bypass ratio, fan noise is a major noise source. Accurate simulation of noise propagation within the engine duct and far-field noise radiation are quite important for the urgent development of silent aircraft. In addition to analytical techniques [1–3], a significant amount of research has been undertaken to develop computational methods for engine noise problems using either frequency domain [4–6] or time domain methods [7–9]. For cases with an axisymmetric mean flow environment, a 2.5-dimensional (2.5-D) linearized Euler equations (LEE) model [7] was developed in previous works [8,10,11] to solve three-dimensional (3-D) problems on a two-dimensional (2-D) domain. The model was validated by comparing its solution to an analytical solution in a half-infinite straight duct case. To avoid numerical instability excited in the downstream shear layer, a modified LEE model was presented by removing a couple of terms in the LEE model [7]. On the other hand, through applying an acoustic filtering on the LEE model, a new model with a set of so-called acoustic perturbation equations (APE) [12,13] has been developed in recent years. The APE model removes vortical modes and thus suppresses numerical instabilities in the sheared flow. In our previous work [8], the APE model was extended for duct cases on a 2-D domain with an axisymmetric mean flow. Compared with the modified LEE model, the physical meaning of the APE model is clear.

Recently the capacity of our proprietary aeroacoustic code was extended for more realistic geometries and flow/acoustic conditions, such as scarf nozzles and engine installation parts. A 3-D APE model was implemented for both Cartesian and cylindrical coordinates. The correctness of the 3-D code implementation was examined by comparing its results with those of the previous 2.5-D APE code in an axisymmetric case, for which an analytical solution [14] is available. The installation effect of bifurcations was subsequently investigated with the newly developed 3-D method. Bifurcations are components used to install an engine on aircraft. The installation of bifurcations can impose influence on the spinning mode propagation pattern and strength [15–17].

The installation effect of bifurcations with the cross section of a NACA 0012 airfoil shape within a generic engine bypass duct was studied previously [15]. A model based on a parabolic approximation of the Helmholtz equation was used. The radiation was predicted at 1.9 m away from the origin of the duct exit. A case with four combined spinning modes ($m = 5, n = 1$), ($m = 5, n = 2$), ($m = 10$, $n = 1$), and ($m = 10$, $n = 2$) at a frequency of 3000 Hz was studied, where m is the circumferential mode and n is the radial mode. It was found that the bifurcations affected sound propagation results. To alleviate the installation effect, a liner treatment on the bifurcation was also investigated. For the similar topic, a 2-D LEE model based on Fourier decomposition in the circumferential direction was used [16]. The technique was applied to a limited number of 2-D planes to save computing time. A flat plate bifurcation was placed in a straight annual duct. A multi-m mode case, from circumferential mode $m = -22$–22, was studied. It was found that mode energy transferred from the $m = 4$ mode to higher or lower modes. A numerical simulation using a finite element method was also performed to study the bifurcation effect [17]. Four modes ($m = 0$, $n = 1$), ($m = 9$, $n = 1$), ($m = 15$, $n = 1$), and ($m = 18$, $n = 1$) at frequencies from 500 to 1000 Hz were studied. Two bifurcations with a rectangular shape were regularly placed in the bypass duct. The study on

Presented as Paper 2877 at the AIAA/CEAS 14th Aeroacoustic Conference, Vancouver, British Columbia, Canada, 5 May–5 August 2008; received 11 July 2008; revision received 14 October 2008; accepted for publication 14 October 2008.

*Research Fellow, Aeronautics and Astronautics, School of Engineering Sciences; x.chen@soton.ac.uk.

†Lecturer, Aeronautics and Astronautics, School of Engineering Sciences; xunger@soton.ac.uk. AIAA Member.

‡Professor, Aeronautics and Astronautics, School of Engineering Sciences; x.zhang1@soton.ac.uk. Associated Fellow AIAA.

thickness of the bifurcation revealed that the thicker the bifurcation, the more energy was reflected. In addition, the liner treatment gave a maximum 2 dB reduction in sound power level.

Those previous works mainly focused either on the demonstration of the computation method or on liner effect. The main objective of this paper is to compare the bifurcation effect in terms of acoustic radiation pattern and strength change. The 3-D APE model was applied to an engine bypass duct with four bifurcations. The installation effect in terms of sound pressure level (SPL) and far-field radiation directivity was studied by comparison to the duct case without bifurcations. As compared with previous works, the major contributions of this paper are 1) the collective effect of the bifurcations was studied at far field, and 2) it was found that the bifurcations scatter acoustic modes and redirect sound propagation. The paper is organized as follows. Section II gives the details of the numerical model. Section III presents and discusses the numerical results for the cases with/without the installation of bifurcations. Finally, Section IV summarizes the present work.

II. Numerical Model

A. Acoustic Perturbation Equations

This research focused on the prediction of propagation and radiation of spinning modes generated by the engine fan and fan/stator flow interactions. As the acoustic perturbation is small compared with the background flow, sound wave propagation can be modeled by LEE. For typical axisymmetrical engine geometry, it is more convenient to formulate LEE in the cylindrical coordinates. Assuming that the acoustic disturbances are restricted to the blade passing frequency and its harmonics, it is possible to write the disturbances at each frequency by a Fourier series in terms of circumferential modes. For instance, a series representing the pressure disturbance p' at a single angular frequency k is

$$p' = \sum_{m=-\infty}^{\infty} p'_m(x, r) e^{[i(kt - m\theta)]} \tag{1}$$

where x is the axial coordinate, r is the radial coordinate, i is the imaginary unit, t is the sound wave propagation time, m is the circumferential mode, and θ is the circumferential angle.

For a generic duct case, the complete governing equations of the 3-D APE model are

$$\begin{aligned}
&\frac{\partial \rho'}{\partial t} + \frac{\partial(\rho' u_0 + \rho_0 u')}{\partial x} + \frac{\partial(\rho' v_0 + \rho_0 v')}{\partial r} + \frac{\partial(\rho' w_0 + \rho_0 w')}{r\partial\theta} \\
&\quad + \frac{\rho' v_0 + \rho_0 v'}{r} = 0, \\
&\frac{\partial u'}{\partial t} + \frac{\partial(u_0 u' + v_0 v' + w_0 w')}{\partial x} + \frac{(\partial p'/\rho_0)}{\partial x} = 0, \\
&\frac{\partial v'}{\partial t} + \frac{\partial(u_0 u' + v_0 v' + w_0 w')}{\partial r} - \frac{2 w_0 w'}{r} + \frac{(\partial p'/\rho_0)}{\partial r} = 0, \\
&\frac{\partial w'}{\partial t} + \frac{\partial(u_0 u' + v_0 v' + w_0 w')}{r\partial\theta} + \frac{v_0 w' + v' w_0}{r} + \frac{(\partial p'/\rho_0)}{r\partial\theta} = 0
\end{aligned} \tag{2}$$

where superscript $'$ and subscript 0 denote perturbation and mean properties, respectively; u, v, and w are velocity components in the x, r, and θ directions of the cylindrical coordinates. Axisymmetrical mean flow was assumed and w_0 was set to zero. The fluid is modeled as a perfect gas with the homentropic assumption: $p' = C_0^2 \rho'$, where C_0 is the sound speed.

A detailed derivation of the APE model on the cylindrical coordinates and discussion of its suitability were given previously [8]. The major interest here is the spinning mode propagation in the near field, refractions in the sheared flow and radiation to the far field. The spinning mode waves were admitted into the computational domain through a buffer zone [7]. The other sound source due to the sheared mean flow was not considered in the current computation [12]. The resultant homogeneous APE [Eq. (2)] are actually perturbation equations introduced by Pierce [18]. The equations can be properly applied only in the high-frequency regime, where the characteristic temporal and spatial scales of the perturbation are much smaller than the corresponding scales of the background flow. The assumption is valid for the present investigation at a frequency of 1547 Hz.

B. Implementation

A quarter of the aft engine duct configuration for a generic engine is illustrated in Fig. 1. The geometry includes bifurcations, the bypass, and exhaust ducts. Four bifurcations are placed along the circumferential direction at regular angle intervals of 90 deg to connect the inner and the outer bypass duct walls. At the duct inlet, the inner wall radius of the exhaust duct is 0.57 m, the exhaust cone radius is 0.23 m, the inner wall of the bypass duct radius is 0.79 m, and the inner hub radius is 0.6 m. In the present computation, the length of the bypass duct from the spinning mode entry area to the duct exit is 4 m. The bifurcations have a cross section of a NACA 0012 airfoil shape with a chord of 1 m. The starting position of the bifurcations is 3 m away from the bypass duct exit. The installation angle for the four bifurcations in the circumferential θ coordinate is 0, 90, 180, and 270 deg, respectively. The installation positions can be easily adjusted later for other specific applications. For the acoustic computations presented next, all variables were nondimensionalized using a reference length of 1 m, a reference density of 1.225 kg/m^3, and a reference sound speed of 346.76 m/s.

The computations were performed on structured grids. The temporal scheme used in the computations is a low-dissipation, low-dispersion Runge–Kutta scheme [19] and the spatial scheme is a sixth-order-accurate compact scheme [20]. An explicit filter of 10th-order accuracy [21] is applied at every time step to remove small numerical disturbances. For the bifurcation case, the grids for acoustic computation consist of 1.27×10^6 cells. The grid resolution has a minimum of nine points per wavelength (PPW) in both directions. In the circumferential direction, a 10 PPW of grid resolution was used to retain accuracy. The computation was performed on a Linux PC cluster using 12 processors with 3.06 GHz clock speed each and 14 GB of memory. A computation of 50 acoustic propagation periods required 40 h computing time for the bifurcation case.

To assess the effect of bifurcations, an axisymmetric bypass duct case (without bifurcations) was also computed. Both 3-D and 2-D grids were constructed for the axisymmetric duct case. The correctness of the newly developed 3-D code was therefore examined on the axisymmetric duct case by comparing to the previous 2-D code with the 2.5-D APE model, whose accuracy was previously validated with several benchmark cases [7,8]. The 3-D grids consist of 0.49×10^6 cells. The required computation time for the simulation was 13 h on the same 12 processors. In contrast, the computation on the 2-D grids that consist of many less cells was quite quick, even on a single processor.

The problem setup is shown in Fig. 2, where only a 2-D plane at $\theta = 90$ deg was displayed for clarity. The inflow and outflow

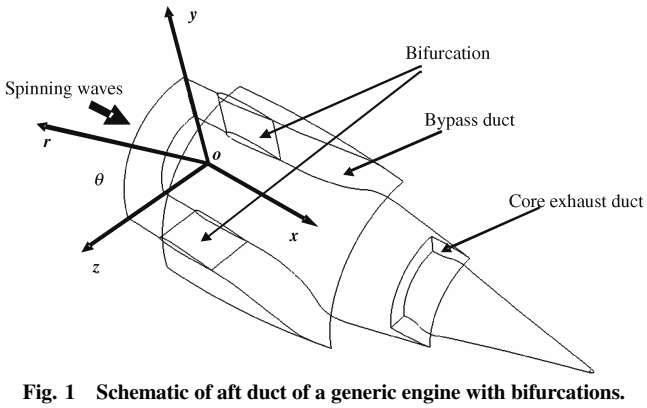

Fig. 1 Schematic of aft duct of a generic engine with bifurcations.

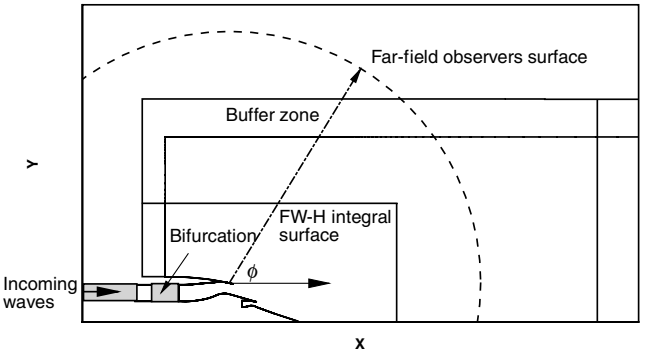

Fig. 2 Setup including bypass duct and exhaust geometry. Geometry is not scaled.

buffer zones [7] were placed in the inflow and outflow areas to minimize possible spurious wave reflections at the computational boundaries. The inflow buffer zone also accommodates spinning mode waves, whose analytical solutions in the straight inflow buffer zone were given previously [7,8]. A periodic boundary condition was applied at the boundaries in the circumferential direction except at the bifurcations. A slip-wall condition was applied to all wall boundaries including the bifurcation boundaries. A symmetric flow condition was applied at the axis. Estimation of far-field acoustic radiation was performed separately based on the near-field computation results through an integral formula of Ffowcs Williams-Hawkings (FW-H) equation [22]. The surface integration was approximated on each panel by midpanel quadrature [23]. The FW-H implementation was previously validated with analytic solutions [7,24]. Comparisons were also made with a finite element/infinite element code for the case of acoustic radiation from an engine intake with a realistic background flow [11]. It was found that the larger the panel number, the better agreement that could be obtained in the interference dip angles. The far-field directivity with respect to the radiation angle ϕ was calculated at 100 units away from the lip of the bypass duct exit. The solutions on the 3-D FW-H integral surface were collected from the 3-D acoustic computation results directly. For the 2-D axisymmetrical case solved by the 2.5-D APE model [8], the 3-D FW-H surface solutions were constructed using Eq. (1). More details of the FW-H implementation were given previously [7,8].

The steady background flow was solved by the Reynolds-averaged Navier–Stokes (RANS) with k-ω turbulence model. Two background mean flows for an axisymmetric bypass duct case and a bifurcation case were solved first. The axisymmetric duct case was used to examine the correctness of the 3-D APE code. The installation effect was subsequently studied by comparing the solutions of the axisymmetric duct case to the bifurcation case. For both axisymmetric and bifurcation duct cases, the inflow conditions were as follows: a pressure of 112,058 Pa and a Mach number of 0.27 at the bypass duct inlet, and a pressure of 101,325 Pa and a Mach number of zero at the freestream. Temperature was a constant of 299.2 K. The mean pressure and the mean axial velocity (in Mach number) contours for the bifurcation case are shown in Figs. 3 and 4. For clarity, only the 2-D plane at $\theta = 90$ deg is shown in Fig. 4. The mean flow for the axisymmetric duct case was not shown here for the brevity of the paper.

The mean flow data were interpolated onto the acoustic grids with suitable resolution for acoustic computation. The analytical solution assigned in the input buffer zone for the admittance of the spinning waves was only suitable to the mean flow without boundary layer. A more generic solution for a mean flow with boundary layer is unavailable. As a result, the boundary layer has to be removed from the RANS results. That is, the mean flow velocity values were the same in the radial direction at the first three grid points near the duct walls. Otherwise, the mismatch between the idealized mean flow in the input buffer zone and the realistic mean flow leads to numerical instability.

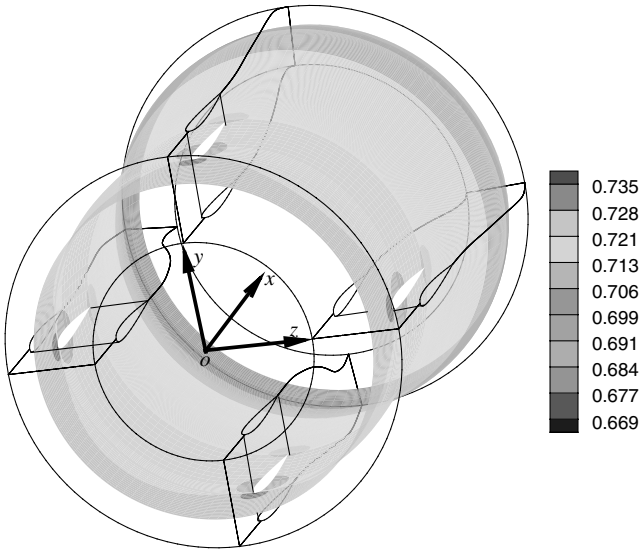

Fig. 3 Mean pressure around bifurcations.

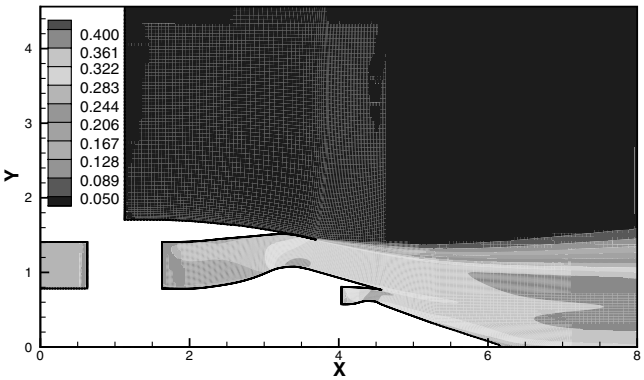

Fig. 4 Mean axial velocity distribution.

C. Code Test

To assess the correctness of the newly developed 3-D APE code, its results were compared with the results of the previous 2.5-D APE code [8] in an axisymmetric duct case for the $(m = 12, n = 1)$ mode. The far-field directivity results of SPL with respect to the radiation angle ϕ is shown in Fig. 5, where the origin for the far-field pattern is at the lip of the bypass duct. The SPL values were calculated with a reference pressure of 2×10^{-5} Pa. It is evident that the 3-D APE results match the 2.5-D APE results with slight angle shifts within main radiation peak range. Two major radiation peaks by the 3-D APE computation are 61.5 dB at 40.0 deg and 60.6 dB at 44.9 deg. On the other hand, the corresponding peak values by the 2.5-D APE

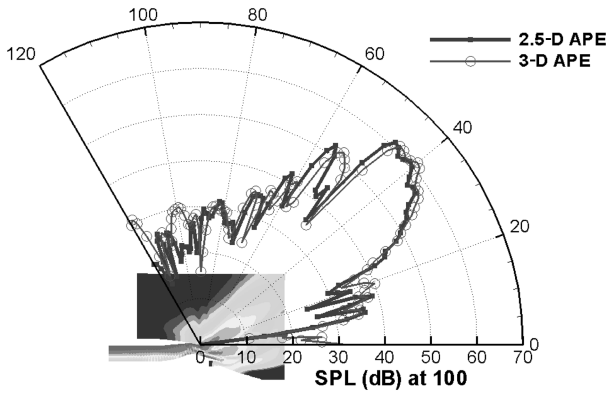

Fig. 5 Far-field directivities by the 2.5-D APE and 3-D APE computations.

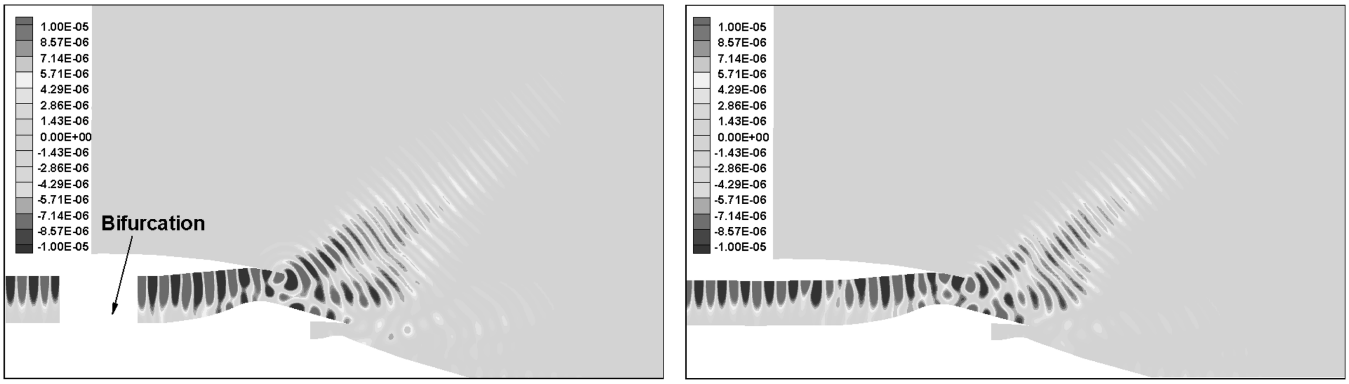

a) b)

Fig. 6 Acoustic pressure contours of 2-D planes at a) $\theta = 0$ deg and b) $\theta = 45$ deg. Single-*n* mode case.

computation are 60.5 dB at 41.2 deg and 61.0 dB at 46.0 deg. The maximum differences are 0.5 dB in the strength and 1.2 deg in the radiation angle. At the first interference dip, the SPL value by the 3-D APE computation is 34.7 dB at 48.5 deg, whereas the result of the 2.5-D APE computation is 35.5 dB at 49.7 deg.

Both computational domains share the same x–y grids. The solutions on the circumferential coordinate were obtained by an analytical relation in 2.5-D APE computation [7,24]. Theoretically, the 2.5-D APE model has an infinite circumferential grid resolution. For practical reasons, 20 PPW of the grid resolution was used to construct a 3-D FW-H integration surface using Eq. (1). For the 3-D APE computation, however, the 3-D grids in the circumferential direction only have 10 PPW of the grid resolution to save computational efforts. The relatively poor grid resolution in the 3-D APE results in numerical dispersion that leads to the differences shown in Fig. 5. As the differences are little, it can be concluded that the 3-D APE implementation is correct.

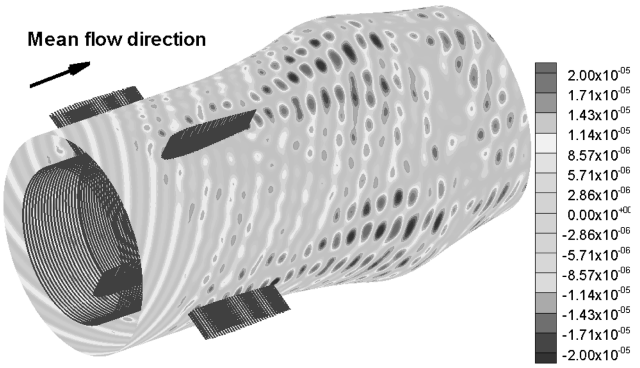

Fig. 7 Acoustic pressures on a cross section of the bifurcation case. Single-*n* mode case.

III. Results of Bifurcation Cases

A. Single-*n* Mode Case

For the single mode case ($m = 12$, $n = 1$), Fig. 6 compares acoustic pressure contours between a middle plane ($\theta = 45$ deg) and a bifurcation plane ($\theta = 0$ deg) along the circumferential direction. It can be seen that the strength of acoustic pressures are increased on the downstream side of the bifurcations due to the scattering. The main radiation peaks are also stronger, although the main radiation peak angles are almost the same for both θ planes.

To show the scattering effect of bifurcations on acoustic pressure redirection, a slice of the acoustic pressure distribution in the x–θ coordinates is shown in Fig. 7. It can be seen that a circumferentially moving mode is diffracted from the bifurcations, which results in stronger acoustic pressures when the diffracted modes interfere with each other behind the bifurcations.

Figure 8 compares the acoustic pressure distributions on a cross section at $x = 5$ for the axisymmetric duct case and the bifurcation case. It is clearly shown that the existence of the bifurcations distorts the acoustic pattern. To study the difference quantitatively, the acoustic pressure distributions on a circle, that is at $x = 5$ and $r = 1.477$ (r is already given in Fig. 1), were compared in Fig. 9. Typically, an incident mode of order m is scattered by the

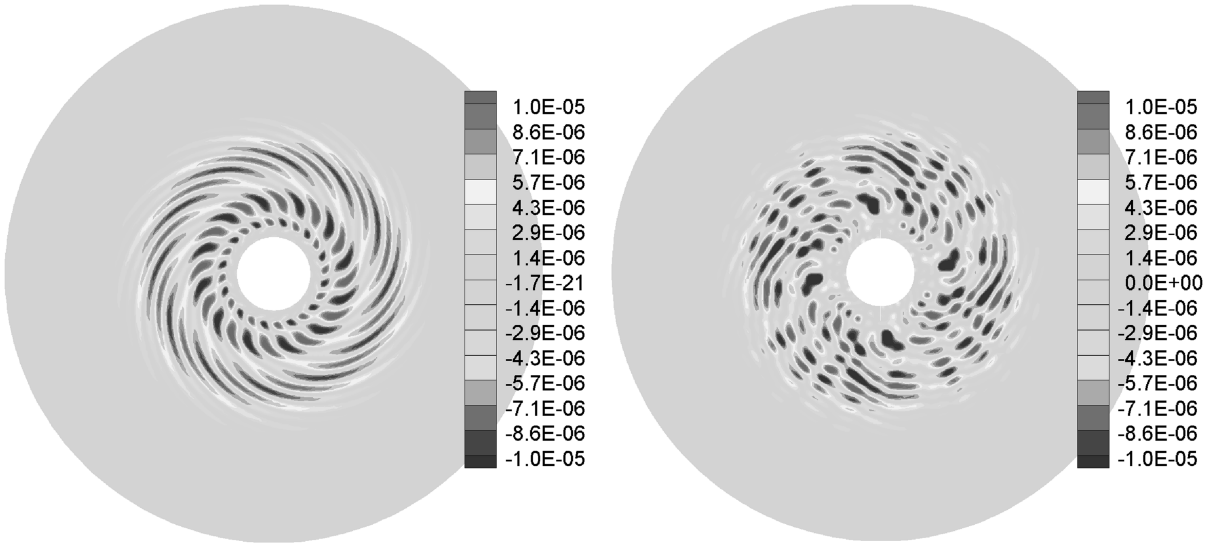

a) b)

Fig. 8 Acoustic pressure patterns on 2-D planes at $x = 5$: a) axisymmetric duct case, and b) bifurcation case. Single-*n* mode case.

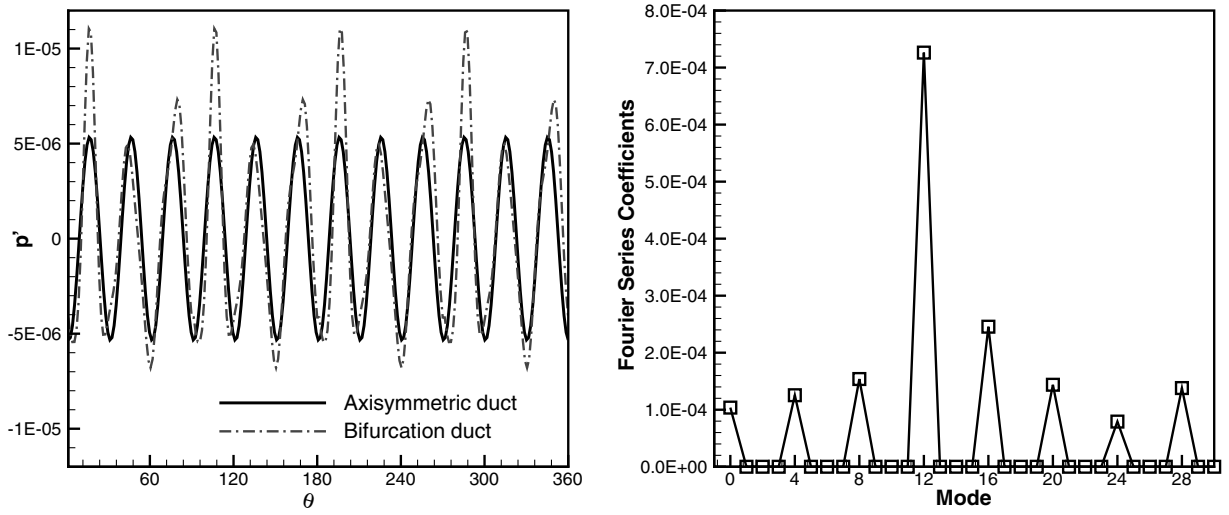

a) b)

Fig. 9 Acoustic pressure distribution: a) with respect to the circumferential angle, and b) its Fourier series analysis results. Single-*n* mode case.

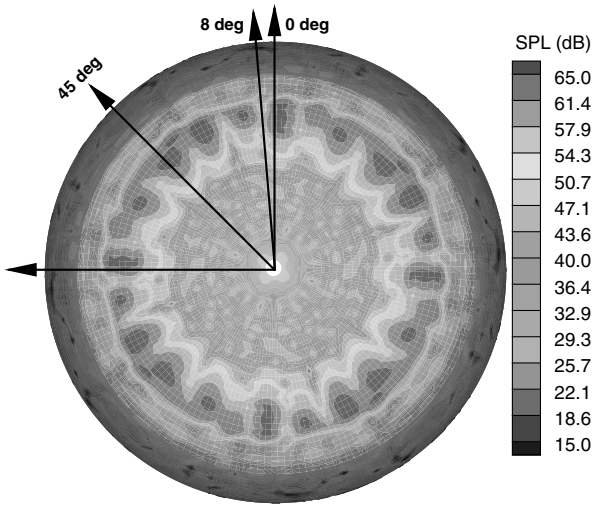

Fig. 10 SPL contours at far field, where 0–45 deg indicate circumferential angles. Single-*n* mode case.

periodically placed bifurcations. The scattering process generates additional modes of orders $m - 4l$, where l is any integer number. The azimuthal pressure profile in Fig. 9a obviously exhibits a residual mode $m = 0$ as an offset and contributions at all multiples $m = 4s$, where s is any integer number. The finding is confirmed by Fourier series analysis, and the coefficient results are shown in Fig. 9b. The results suggest that the original mode $m = 12$ still dominates the whole spectrum. Other than that dominant mode, the bifurcations also produce new modes of the periodicity order of 4, where the symmetric mode $m = 0$ is responsible for a nonzero radiation near the x axis.

A 2-D projection of the 3-D far-field SPL pattern at 100 units is shown in Fig. 10. The outward face of the hemisphere centered at $\phi = 0$ and $\theta = 0$ was displayed. A total number of 10,860 observer positions were calculated with a resolution of 2 deg in both the circumferential $(0 < \theta \leq 360$ deg) and radiation angle $(0 < \phi \leq 120$ deg) directions. The lobed structure of the figure indicates that an equivalent standing-wave pattern in the azimuthal direction is formed, in contrast with the axisymmetric duct case for which the SPL would be axisymmetric.

The individual far-field directivity profiles were compared at two cross sections ($\theta = 0$ and 45 deg) in Fig. 11a. Comparing those with the axisymmetric duct case, it can be found that the peak radiation angles remain the same. The angle range of peak radiation is from $\phi = 33$ to 48 deg. Two maximum SPL values of 63.0 and 62.5 dB were observed for the $\theta = 0$ deg cross section at radiation angles of $\phi = 41.2$ and 44.9 deg, respectively. One maximum SPL value of 63.8 dB at a radiation angle of $\phi = 41.6$ deg was observed for the $\theta = 45$ deg cross section. For the axisymmetric duct case, two maximum SPL values of 60.3 and 60.6 dB were observed for the $\theta = 0$ deg cross section, at radiation angles of $\phi = 41.2$ and 44.8 deg, respectively. Compared to the axisymmetric duct case, there is a maximally 3.2 dB increase in SPL for the bifurcation case

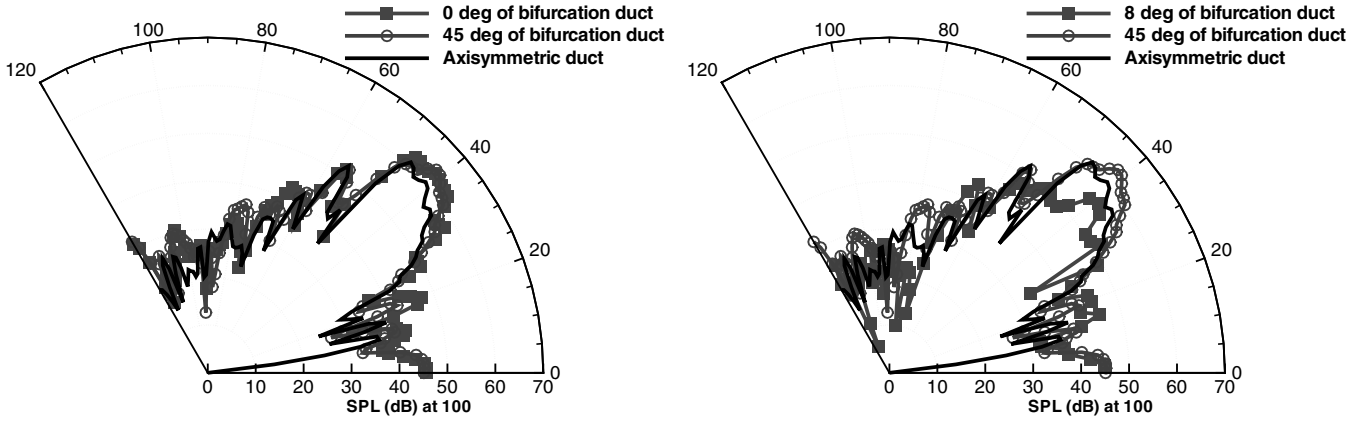

a) b)

Fig. 11 Far-field directivities. Single-*n* mode case.

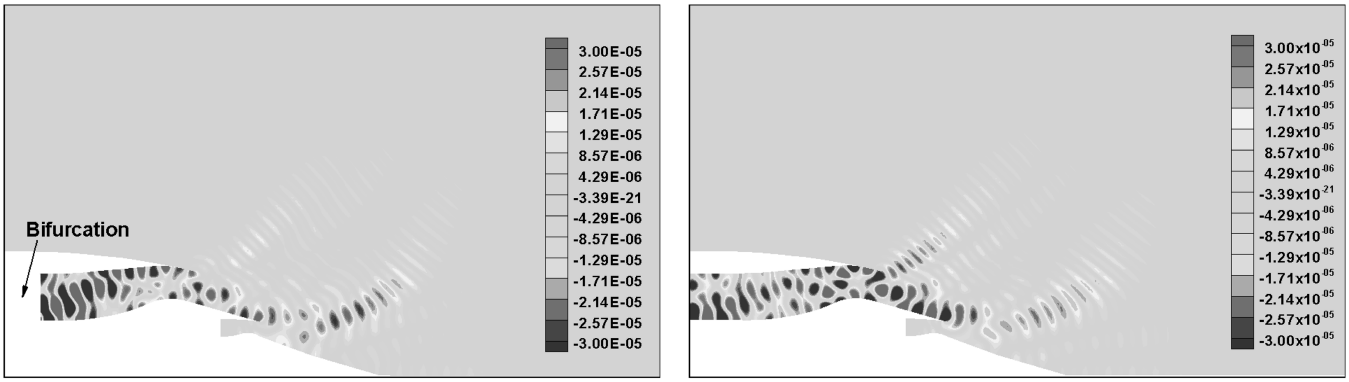

a) b)

Fig. 12 Acoustic pressure contours of 2-D planes at a) $\theta = 0$ deg and b) $\theta = 45$ deg. Multi-n mode case.

due to the scattering. In addition, higher sound pressure levels are found in lower radiation angles (from $\phi = 0$ to 20 deg). As discussed previously, the nonzero radiation on these low radiation angles is caused by the asymmetric mode $m = 0$.

The azimuthal angles $\theta = 0$ and 45 deg chosen in Fig. 11a coincide with the local maxima lobes in Fig. 10. Hence, both far-field directivity patterns at the two azimuthal planes in Fig. 11a are similar in terms of the amplitude and radiation angle of peaks. Figure 11b shows the far-field directivity pattern at an extinction plane with the azimuthal angle $\theta = 8$ deg (Fig. 10). Compared to the axisymmetric duct case and the bifurcation case at one of the local maxima planes ($\theta = 45$ deg), there is a 4–7 dB reduction in SPL for the bifurcation case at the extinction plane ($\theta = 8$ deg). In lower radiation angles, higher sound pressure levels can still be found. Figure 11 suggests that the bifurcations do not generate noise but redirect sound radiation from the duct. The noise is reduced at some azimuthal planes but is increased elsewhere. It is worth noting that, for practical applications, the local noise enhancement is a major drawback attributed to the technology of the bifurcations.

B. Multi-n Mode Case

The multi-n mode case contains radial modes from $n = 1$ to 5. The circumferential mode is still $m = 12$. For the single radial mode case, complex acoustic propagation patterns and mode interference appear for the multi-n mode case. In observing the acoustic pressure distribution at the middle plane ($\theta = 45$ deg) and the bifurcation plane ($\theta = 0$ deg) shown in Fig. 12, it is noticed that the stronger acoustic pressures appear behind the bifurcations. They also appear

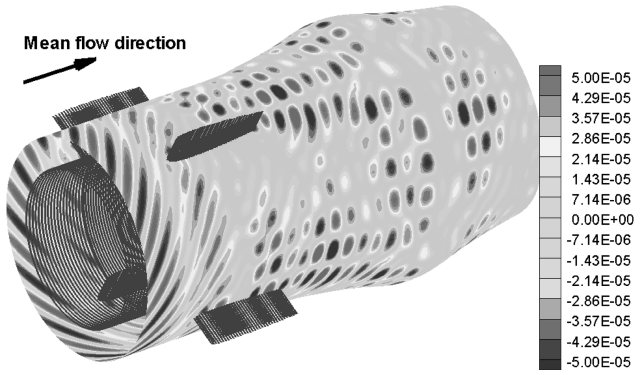

Fig. 13 Acoustic pressures on a cross section of the bifurcation case. Multi-n mode case.

over the external surface of the core nozzle in the middle plane. Behind the bifurcations, strong acoustic modes are reflected from the edge of the bypass duct, resulting in a stronger radiation pattern at lower radiation angles. A plane view (x–θ plane) was given in Fig. 13 to examine the acoustic pressure distributions more clearly. It can be seen that a complex pattern was formed behind the bifurcations.

Similar to the single mode case, the acoustic pressure contours on a cross section at $x = 5$ clearly show the bifurcation effect again. Figure 14 shows that the existence of the bifurcations distorts the multi-n mode acoustic pattern. The distortion was quantified on the circle ($x = 5$ and $r = 1.477$) again. Compared to the single mode

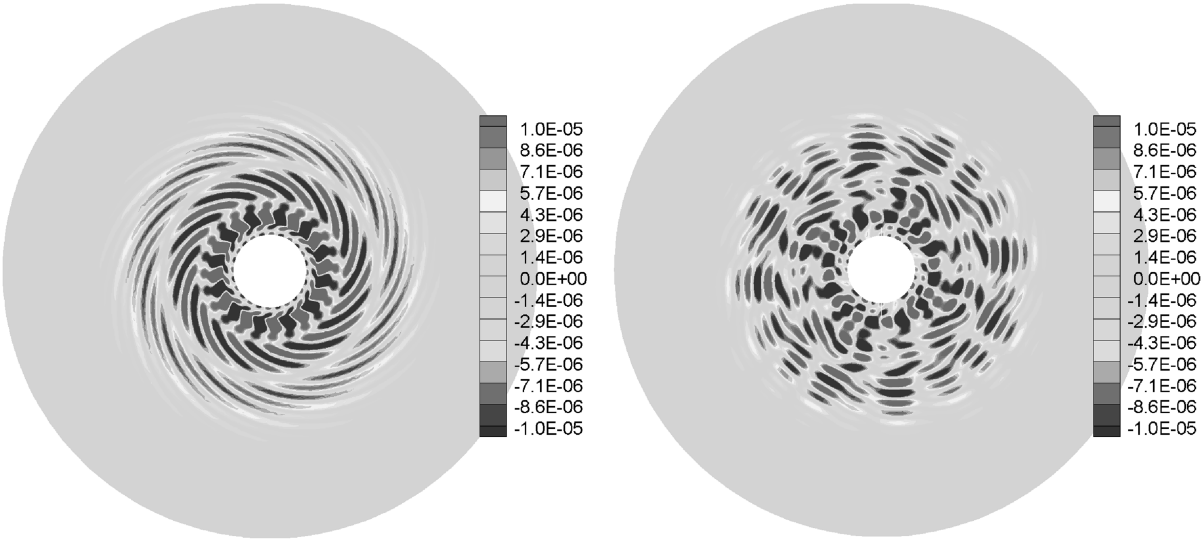

a) b)

Fig. 14 Acoustic pressure patterns on 2-D planes at $x = 5$: a) axisymmetric duct case, and b) bifurcation case. Multi-n mode case.

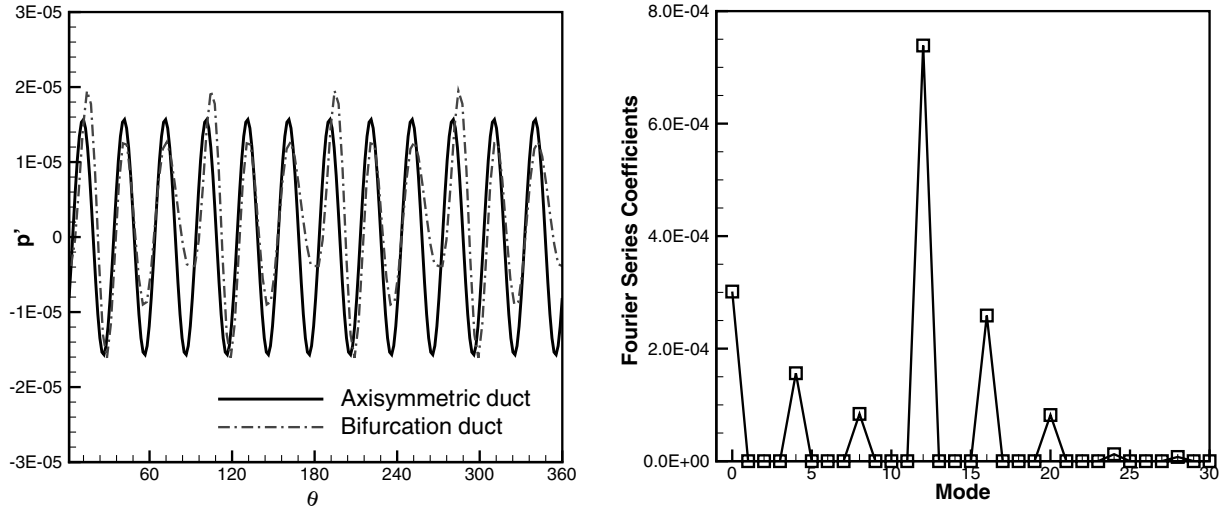

a) b)

Fig. 15 Acoustic pressure distribution: a) with respect to the circumferential angle, and b) its Fourier series analysis results. Multi-*n* mode case.

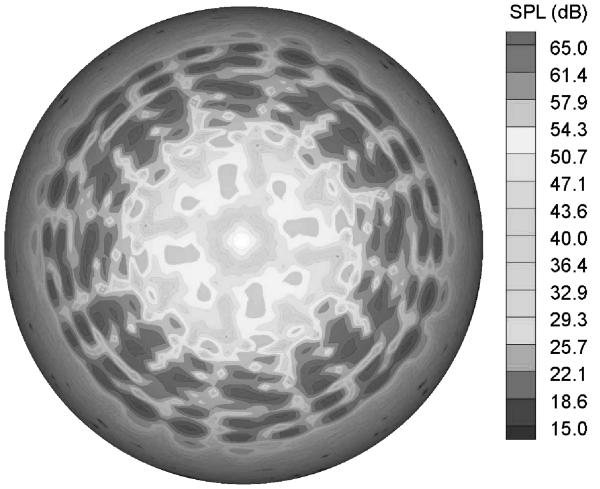

Fig. 16 SPL contours at far field. Multi-*n* mode case.

case, the increase of the pressure amplitudes due to scattering from the bifurcations is less. Figure 15 shows that the amplitude is even reduced at some circumferential angles. Compared with the Fourier series analysis results for the single-*n* case in Fig. 9b, Fig. 15b shows the asymmetric mode $m = 0$ becomes larger. It suggests that the noise radiation of the multi-*n* case will be stronger than the noise radiation of the single-*n* case in the low radiation angles.

The collective effects of the bifurcations should be studied at far field by the FW-H technique. Figure 16 shows the SPL contours at far field. Again, a complex radiation pattern can be observed, suggesting the bifurcation effect. There are additional modes appearing at the lower radiation angles compared with the axisymmetric duct case (Fig. 17). The bifurcations scatter and redirect the acoustic modes. As a result, the sound level at far field was affected. The first radiation peak has a maximum value of 68.5 dB at $\phi = 39.8$ deg. In comparison with the counterpart in the axisymmetric duct case (66.5 dB at $\phi = 39.8$ deg), there is an increase of 2.0 dB. Compared with Fig. 11, Fig. 17 shows that the multi-*n* mode case was affected more than the single-*n* case, especially within the low radiation angles from 0 to 50 deg, which is consistent with the previous finding by Fourier series analysis.

IV. Conclusions

The investigation was performed on the case with four bifurcation arrangements regularly placed in the circumferential direction of the bypass duct. Although only the results for a couple of modal combinations are given, the findings for other modes at high frequency are similar. Its computational results were compared with those of the axisymmetric duct case. In comparison with previous works on the bifurcation effect, this work confirmed that the bifurcations have influences on the near-field sound pressures through quantitative comparisons with the axisymmetric duct case. In the near field, for the single-*n* mode case, the bifurcations scatter acoustic modes resulting in the increase of the peak amplitude of acoustic waves. The peak radiation angles are still the same. For the

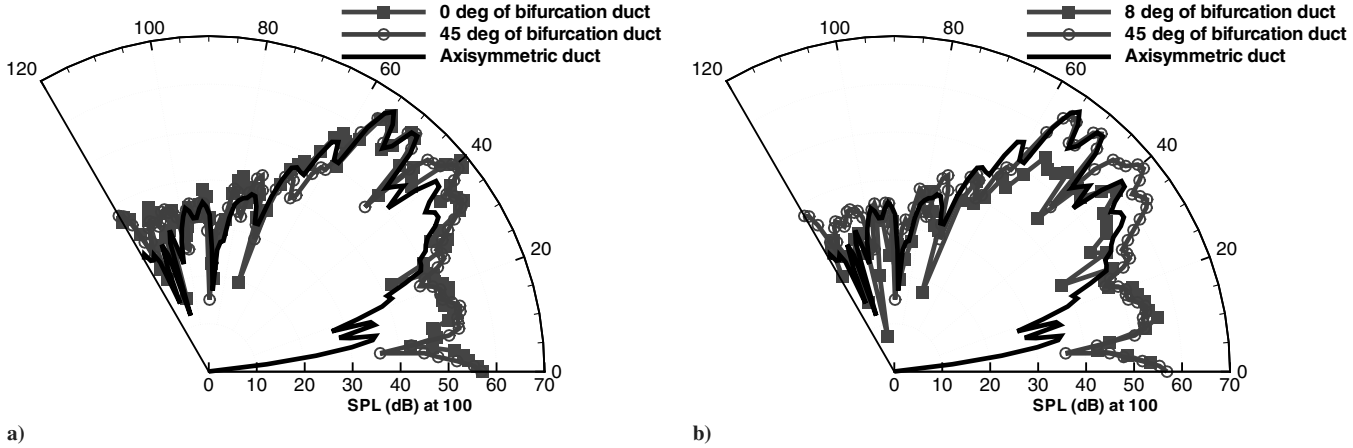

a) b)

Fig. 17 Far-field directivities. Multi-*n* mode case.

multi-n modes case, additional radiation peaks appear at low radiation angles. In addition to the acoustic scattering, the amplitude of sound waves is also increased after the bifurcations. Furthermore, the influence of the bifurcations on far-field radiation angle and strength were also studied by the FW-H solver. Compared with the near-field results, far-field results show the difference between axisymmetric duct cases and bifurcation cases more clearly. In the far field, for the bifurcation duct case, the main radiation peaks are shifted to lower radiation angles for both single- and multi-n mode cases by the bifurcation arrangements. In addition, there are additional radiation peaks appearing at the lower radiation angles. Furthermore, the levels of the sound pressures at the far field are increased, especially for the multi-n case at low radiation angles. In summary, through the investigation, the effects of the bifurcations on spinning mode sound radiation from the generic engine bypass duct are studied and revealed. The current method should also be applicable to other configurations with different bifurcations and modes.

References

[1] Ovenden, N. C., and Rienstra, S. W., "Mode-Matching Strategies in Slowly Varying Engine Ducts," *AIAA Journal*, Vol. 42, No. 9, 2004, pp. 1832–1840. doi:10.2514/1.3253

[2] Gabard, G., Astley, R. J., and Tahar, M. B., "Noise Radiation from a Jet Pipe: A Benchmark Problem for Computational Aeroacoustics," AIAA Paper 2005-3064, 2005.

[3] Gabard, G., and Astley, R. J., "Theoretical Model for Sound Radiation from Annular Jet Pipes: Far- and Near-Field Solutions," *Journal of Fluid Mechanics*, Vol. 549, 2006, pp. 315–341. doi:10.1017/S0022112005008037

[4] Eversman, W., and Okunbor, D., "Aft Fan Duct Acoustic Radiation," *Journal of Sound and Vibration*, Vol. 213, No. 2, 1998, pp. 235–257. doi:10.1006/jsvi.1997.1480

[5] Casalino, D., and Genito, M., "Turbofan Aft Noise Predictions Based on Lilley's Wave Model," *AIAA Journal*, Vol. 46, No. 1, 2008, pp. 84–93. doi:10.2514/1.32046

[6] Casalino, D., and Genito, M., "Achievements in the Numerical Modeling of Fan Noise Radiation from Aero-Engines," *Aerospace Science and Technology*, Vol. 12, No. 1, 2008, pp. 105–113. doi:10.1016/j.ast.2007.10.005

[7] Zhang, X., Chen, X. X., Morfey, C. L., and Nelson, P. A., "Computation of Spinning Modal Radiation from an Unflanged Duct," *AIAA Journal*, Vol. 42, No. 9, 2004, pp. 1795–1801. doi:10.2514/1.890

[8] Huang, X., Chen, X. X., Ma, Z. K., and Zhang, X., "Efficient Computation of Spinning Modal Radiation Through an Engine Bypass Duct," *AIAA Journal*, Vol. 46, No. 6, 2008, pp. 1413–1423. doi:10.2514/1.31136

[9] Bogey, C., Bailly, C., and Juvé, D., "Computation of Flow Noise Using Source Terms in Linearized Euler's Equations," *AIAA Journal*, Vol. 40, No. 2, 2002, pp. 235–243. doi:10.2514/2.1665

[10] Richards, S. K., Chen, X. X., Huang, X., and Zhang, X., "Computation of Fan Noise Radiation Through an Engine Exhaust Geometry with Flow," *International Journal of Aeroacoustics*, Vol. 6, No. 3, 2007, pp. 223–241. doi:10.1260/147547207782419534

[11] Huang, X., Zhang, X., and Richards, S. K., "Adaptive Mesh Refinement Computation of Acoustic Radiation from an Engine Intake," *Aerospace Science and Technology*, Vol. 12, No. 5, 2008, pp. 418–426. doi:10.1016/j.ast.2007.09.004

[12] Ewert, R., and Schröder, W., "Acoustic Perturbation Equations Based on Flow Decomposition via Source Filtering," *Journal of Computational Physics*, Vol. 188, No. 2, 2003, pp. 365–398. doi:10.1016/S0021-9991(03)00168-2

[13] Ewert, R., and Schröder, W., "On the Simulation of Trailing Edge Noise with a Hybrid LES/APE Method," *Journal of Sound and Vibration*, Vol. 270, No. 3, 2004, pp. 509–524. doi:10.1016/j.jsv.2003.09.047

[14] Munt, R. M., "The Interaction of Sound with a Subsonic Jet Issuing from a Semi-infinite Cylindrical Pipe," *Journal of Fluid Mechanics*, Vol. 83, 1977, pp. 609–640. doi:10.1017/S0022112077001384

[15] Nark, D. M., Farassat, F., Pope, S., and Vatsa, V., "Effects of Bifurcations on Aft-fan Engine Nacelle Noise," AIAA Paper 2004-2988, 2004.

[16] Baralon, S., Eriksson, L. E., Billson, M., and Andersson, N., "Evaluation of Advanced Prediction Methods for Aero Engine Exhaust Noise," International Symposium on Air Breathing Engines Paper 2005-1190, 2005.

[17] Sugimoto, R., Astley, R. J., Gabard, G., and Tsuchiya, N., "Three-Dimensional Effects of Geometries and Acoustic Treatments on Bypass-Duct Noise," AIAA Paper 2007-3549, 2007.

[18] Pierce, A. D., "Wave Equation for Sound in Fluids with Unsteady Inhomogeneous Flow," *Journal of the Acoustical Society of America*, Vol. 87, No. 6, 1990, pp. 2292–2299. doi:10.1121/1.399073

[19] Hu, F. Q., Hussaini, M. Y., and Manthey, J., "Low-Dissipation and Low-Dispersion Runge-Kutta Schemes for Computational Acoustics," *Journal of Computational Physics*, Vol. 124, No. 1, 1996, pp. 177–191. doi:10.1006/jcph.1996.0052

[20] Ashcroft, G., and Zhang, X., "Optimized Prefactored Compact Schemes," *Journal of Computational Physics*, Vol. 190, No. 2, 2003, pp. 459–477. doi:10.1016/S0021-9991(03)00293-6

[21] Kennedy, C. A., and Carpenter, M. H., "Comparison of Several Numerical Methods for Simulation of Compressible Shear Layers," NASA TP 3484, 1997.

[22] Farassat, F., and Succi, G. P., "The Prediction of Helicopter Rotor Discrete Frequency Noise," *Vertica*, Vol. 7, No. 4, 1983, pp. 309–320.

[23] Brentner, K. S., "Numerical Algorithms for Acoustic Integrals with Examples for Rotor Noise Prediction," *AIAA Journal*, Vol. 35, No. 4, 1997, pp. 625–630. doi:10.2514/2.182

[24] Zhang, X., Chen, X. X., and Morfey, C. L., "Acoustic Radiation from a Semi-infinite Duct with a Subsonic Jet," *International Journal of Aeroacoustics*, Vol. 4, Nos. 1–2, 2005, pp. 169–184. doi:10.1260/1475472053730075

C. Bailly
Associate Editor